Geophys. J. Int. (2000) **143,** 837–846

New seismotectonic data from an intraplate region: focal mechanisms in the Armorican Massif (northwestern France)

D. Amorèse,[1] A. Walker,[2] J.-L. Lagarde,[1] J.-P. Santoire,[3] P. Volant,[4] M. Font[1] and M. Lecornu[5]

[1] *Morphodynamique Continentale et Côtière* (M2C) UMR CNRS 6143, *Université de Caen,* 14032 *Caen Cedex, France. E-mails: amorese@geos.unicaen.fr; lagarde@geos.unicaen.fr; font@geos.unicaen.fr*

[2] *British Geological Survey, Murchison House, West Mains Road, Edinburgh,* EH9 3LA, *UK. E-mail: abw@wpo.nerc.ac.uk*

[3] *Laboratoire de Détection et de Géophysique,* BP 12, F91680 *Bruyères-Le-Châtel, France. E-mail: santoire@ldg.bruyeres.cea.fr*

[4] *Institut de Protection et de Sûreté Nucléaire, Bureau d'Evaluation des Risques Sismiques pour la Sûreté des Installations Nucléaires,* 60–68 *avenue du Général Leclerc,* BP 6, 92265 *Fontenay-Aux-Roses Cedex, France. E-mail: philippe.volant@ipsn.fr*

[5] *Ecole et Observatoire de Physique du Globe,* 5 *rue Descartes,* F-67084 *Strasbourg Cedex, France. E-mail: marianne.lecornu@sirius.u-strasbg.fr*

Accepted 2000 July 14. Received 2000 July 13; in original form 1999 December 20

Downloaded from https://academic.oup.com/gji/article/143/3/837/721582 by guest on 10 January 2021

SUMMARY

Focal mechanism solutions are determined for 11 small intraplate earthquakes that occurred between 1990 and 1998 in Normandy and the Channel Islands. These mechanisms are obtained from the *P*-wave first-motion polarities recorded by stations from local and regional seismic networks. The accuracy of each hypocentral location is closely examined and the quality of each fault plane solution is discussed by considering the influence of the velocity structure. The predominant feature of the computed focal mechanisms is the relatively widespread near-horizontal NE–SW T-axis orientation. Horizontal P-axes strike roughly NW–SE. Mechanism solutions for the earthquakes in the Avranches region show left-lateral strike slip on a NNW–SSE fault zone. For the overall region, it seems that nodal planes of normal faulting solutions trend NW–SE or WNW–ESE, whereas those of thrust faulting solutions trend NE–SW. This is in agreement with the general regional stress pattern. The NE–SW normal fault plane solution of the 1990 Jersey event is unique because it is not consistent with the regional style of faulting.

Key words: fault plane solutions, Jersey, Normandy, seismicity, seismotectonics.

1 INTRODUCTION

The studied region covers the northeastern end of the Armorican Massif (Fig. 1). The seismotectonic pattern of this region is poorly known because this is (i) a region of low tectonic activity and (ii) a region where seismograph stations are poorly distributed (Fig. 1). Thus, in this region the number of available focal solutions is small. Indeed, the low availability of the raw data (first-motion polarities), distributed both over French and British seismological agencies, hinders the compilation of a fault plane solution catalogue. This study is an attempt to overcome these difficulties and obtain at least a simple model of the seismotectonic regime of the eastern part of the Armorican Massif. Our results update the synthetic studies that have already been published on the seismotectonics of France (Nicolas *et al*. 1990; Grellet *et al*. 1993). New data are also produced for the fault plane solutions of some seismic events of the English Channel near the Channel Islands. They complement a study previously published by Walker (1991) on Jersey's seismicity.

2 DATA

The first-motion polarities used in this work are mainly produced by stations belonging to three separate seismic networks (Fig. 1): (i) the LDG/DASE/CEA network (French Atomic Agency), (ii) the BGS network (British Geological Survey) and (iii) the 'Siscaen' network (University of Caen, Normandy). Additional arrival times and polarities provided by the ReNaSS (French National Seismic Network) are also used for locating the seismic events and computing some focal solutions.

The present study updates the work of Nicolas *et al*. (1990), Delouis *et al*. (1993) and Grellet *et al*. (1993); therefore, our computations consider only seismic events after 1989. In order to calculate reliable fault plane solutions, it is necessary to use a threshold number of records (first-motion polarities) per event, thus our study does not consider $M_L < 3$ events: it is thought that the distribution of stations is too sparse to provide enough records for each event with local magnitude smaller than 3. Between 1990 and 1998, the LDG reported 11 $M_L \geq 3$ events in the area studied (2.6°W–0°E; 48.4°N–50°N) (Table 1).

© 2000 RAS

Table 1. List of seismic events with $M_L \geq 3.0$ that occurred between 48.4°N and 50°N and 2.6°W and 0.0°E during the period 1990–1998. These parameters are extracted from the DASE/LDG bulletin, except for the 1990 April 30 event (marked by an asterisk), for which they are from Walker (1991).

Date (Mo/Dy/Yr)	Time	Lat (°)	Lon (°)	M_L	Location
04/30/1990*	23:35:57.3	49.13	−2.13	3.5	Jersey
11/08/1990	18:21:46.2	48.489	−1.481	3.0	Pontorson
07/26/1993	18:52:23.4	48.756	−1.091	3.5	SW Vire
09/17/1994	06:05:06.0	48.966	−2.517	3.4	W Minquiers
11/30/1994	16:31:21.5	49.436	−0.527	4.1	Arromanches
04/22/1995	13:10:14.3	48.635	−2.310	3.5	N Saint-Brieuc
06/01/1996	12:29:23.7	49.339	−1.329	3.0	Saint-Lô
11/26/1996	20:21:35.4	48.696	−1.524	3.9	Avranches
06/22/1997	16:50:16.3	49.204	−2.295	3.4	Jersey
08/08/1998	10:36:16.1	49.265	−0.571	3.5	Caen
12/07/1998	00:23:28.4	48.577	−1.659	3.3	Avranches

Finally, fault plane solutions have been produced for all of these events.

3 FAULT PLANE SOLUTION DETERMINATION

3.1 Fault plane solutions and velocity model

Fault plane solutions are usually strongly influenced by the velocity model used for their computation. The velocity structure under the eastern part of the Armorican Massif is poorly determined. Therefore, there are problems in obtaining a realistic velocity model for locating the seismic events and computing the fault plane solutions. The Moho under the Cadomian block occurs at depths of between 35 and 37 km (Matte & Hirn 1988). Moreover, a recent refraction experiment between northern Brittany and the Channel Islands revealed the following structure (Grandjean *et al.* 2000): the mean crustal velocity ranges from 5.5 to 6.8 km s^{-1} at 15 km depth; lower crustal velocities range from 7.0 to 7.5 km s^{-1} at a depth of 35–38 km and then from 7.5 to 8.1 km s^{-1} at the crust–mantle boundary located between 35 and 38 km depth. Thus, using these observations, we adopt the tabular velocity structure presented in Table 2. The adopted V_P/V_S ratio (1.73) was computed from a Wadati diagram by Walker 1991) for the 1990 Jersey event. Hereafter, the structure that is presented in Table 2 is called the NBCI (Northern Brittany and Channel Islands) velocity model.

The computations (event locations and fault plane solution determinations) have not been restricted by the NBCI velocity model (Table 2) and therefore each event has been processed using both the NBCI and BGS models (Table 3).

The reference velocity model used in this study (Table 2) is, however, particularly relevant for the Armorican Massif; therefore, the use of seismological stations located outside this area may strongly bias the locations of the seismic events. In this study, HYPOCENTER 3.0 (Lienert *et al.* 1986; Lienert & Havskov 1995) is used for locating the earthquakes. It is possible to reduce the influence of far stations by applying an appropriate distance weighting to the data. Here we adopt 200 and 300 km as X_{near} and X_{far} values, respectively [X_{near} and X_{far} are used to calculate the distance weight, w_d,

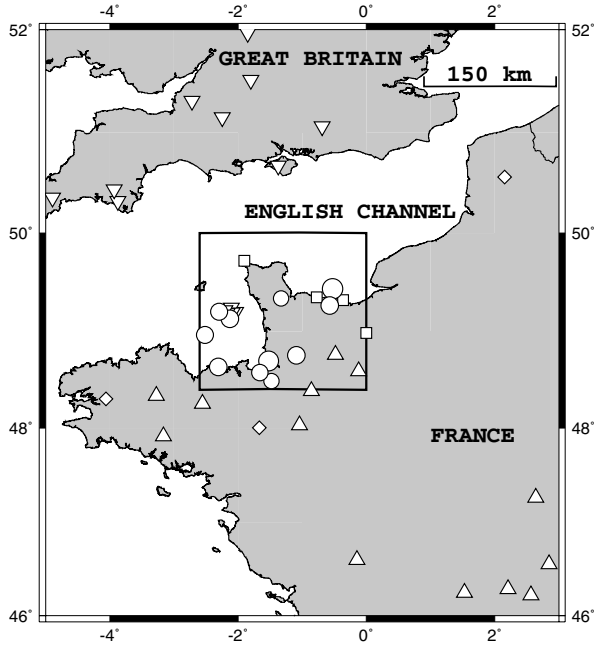

Figure 1. Map showing the region studied (outlined in black).

Table 2. NBCI velocity structure. M in the depth column signifies the Moho for Moho phases (P_n or S_n).

P-wave velocity (km s^{-1})	Depth to top of layer (km)
5.50	0.00
6.20	5.00
6.70	15.00
7.50	35.00 M
8.20	40.00

$V_P/V_S = 1.73$, $X_{near} = 200$ km, $X_{far} = 300$ km

Downloaded from https://academic.oup.com/gji/article/143/3/837/721582 by guest on 10 January 2021

Table 3. BGS velocity structure. M in the depth column signifies the Moho for Moho phases (P_n or S_n).

P-wave velocity (km s^{-1})	Depth to top of layer (km)
4.00	0.00
5.90	2.52
6.45	7.55
7.00	18.87
8.00	34.15 ~ M

$V_P/V_S = 1.73$, $X_{near} = 200$ km, $X_{far} = 300$ km

using $w_d = (X_{far} - \Delta)/(X_{far} - X_{near})$, where Δ is the epicentral distance]. Arrival times of stations beyond 300 km epicentral distance are therefore not considered for event locations: the use of a regional velocity model is then consistent with the data. This restriction does not concern the first-motion polarities. When locating the events, first arrival times are assigned a weight of 1 and late arrival times are assigned a weight of 0.5.

Fault plane solutions are computed with FPFIT (Reasenberg & Oppenheimer 1985) using the polarities of the first seismic phase first motions. The quality of each fault plane solution can be estimated from (i) the total number of first-motion polarities, (ii) the misfit value (this value is an indication of inconsistent polarities) and (iii) the station distribution ratio (Table 5).

The station distribution ratio is expressed as

$$\mathrm{STDR} = \frac{\sum_k (W_0^{j,k} W_t^{i,k})}{\sum_k W_0^{j,k}},$$

where $W_0^{j,k}$ is the weight assigned to the polarity observed at station k for event j and $W_0^{i,k}$ is a weight dependent on the theoretical amplitude of the P wave computed at station k for source model i. When the STDR value is smaller than 0.5, the fault plane solution is possibly unreliable because many data lie near nodal planes.

In this paper, an additional parameter, which we call the similarity coefficient (SC), is computed. This parameter indicates whether multiple solutions for the same event are similar. The similarity coefficient for two fault plane solutions is computed by superimposing the two focal spheres. If the two focal mechanisms are perfectly superimposable (shaded quadrants do not overlap blank quadrants and vice versa), the similarity coefficient is equal to 1. If the two focal mechanisms are perfectly antagonistic, the SC is equal to 0 (Fig. 2). For a given earthquake, similarity coefficients can be computed as follows:

(i) within a group of fault plane solutions obtained using the same velocity structure (multiple solutions automatically computed by FPFIT and corresponding to relative minima in misfit);

(ii) within a group of fault plane solutions obtained using different velocity structures (alternative solutions).

For each earthquake studied in this paper, minimum SC values are computed both for the multiple solutions and for alternative solutions (Table 4). Computing fault plane solutions with different velocity structures is not meaningless: frequently,

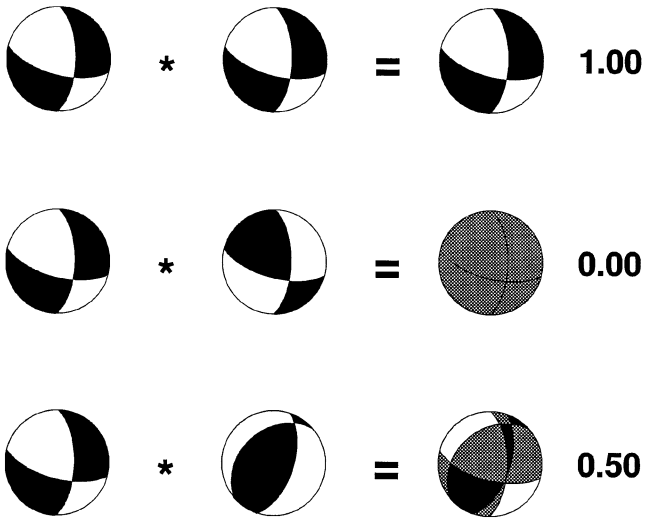

Figure 2. Principle of computation of the similarity coefficient (SC). Focal spheres are superimposed. The similarity coefficient is defined as follows: SC = 1 − (grey area)/(total area). When focal mechanisms are identical (upper part of the figure), the similarity coefficient is equal to 1 (no grey area on the resulting sphere). When focal mechanisms are antagonistic (middle part of the figure), the similarity coefficient is equal to 0 (the whole resulting sphere is grey). In the lower part of the figure, an intermediate layout is shown (SC = 0.5).

Table 4. Minimal similarity coefficient (SC) values for the 11 earthquakes studied. Similarity coefficients are computed between multiple solutions obtained for the NBCI velocity structure (NBCI × NBCI), multiple solutions obtained for the BGS velocity structure (BGS × BGS) and between solutions obtained for the NBCI and BGS velocity structures (NBCI × BGS).

Date (Mo/Dy/Yr)	Location	SC (NBCI × NBCI)	SC (BGS × BGS)	SC (NBCI × BGS)
04/30/1990	Jersey	1.00	0.68	0.75
11/08/1990	Pontorson	1.00	1.00	>0.99
07/26/1993	SW Vire	1.00	1.00	0.58
09/17/1994	W Minquiers	1.00	0.65	0.71
11/30/1994	Arromanches	1.00	1.00	0.77
04/22/1995	Saint-Brieuc	0.44	0.42	0.42
06/01/1996	Saint-Lô	1.00	0.45	0.51
11/26/1996	Avranches	1.00	1.00	0.85
06/22/1997	Jersey	0.42	1.00	0.40
08/08/1998	Caen	0.84	0.87	0.84
12/07/1998	Avranches	0.81	0.54	0.59

Downloaded from https://academic.oup.com/gji/article/143/3/837/721582 by guest on 10 January 2021

for a given earthquake, the use of different velocity structures can lead to significantly varying fault plane solutions (this is illustrated by minimum SC values smaller than or equal to 0.5 in the last column of Table 4). When very different fault plane solutions are obtained for a given earthquake, we have to choose which of the multiple solutions is the 'best' one. Usually, we give preference to solutions with the smallest misfit value. Multiple solutions in agreement (when considering the strain pattern) with the solutions for the other earthquakes are also favoured.

3.2 Fault plane solutions and hypocentral depths

Reliable determination of the hypocentral depth is a prerequisite before any conclusive computation of a fault plane solution. Then, before presenting any results, we address the quality of the hypocentre locations.

In general, any location algorithm is in every way more stable and the hypocentral solution better constrained if P and S arrivals are available at few stations than if P arrivals only are available at many stations (Buland 1976). The addition of S information improves the reliability of the locations and reduces the standard errors of the location parameters (James *et al*. 1969). In this study, we use S arrival times when locating events. Nevertheless, this provision does not ensure reliable focal depth estimates: in the usual iterative least-squares location technique, focal depth can be traded for origin time (Nordquist 1962) unless the studied earthquake occurs close to one of the stations. The rough rule is that any focal depth less than the nearest station epicentral distance will be inaccurate. This condition is not met by most of the earthquakes studied (Table 5), but the proposed hypocentral solutions are certainly not entirely unresolved because (1) the ability of HYPOCENTER to locate shallow distant events accurately has already been demonstrated (Lienert 1997) and (2) it is possible to obtain reliable estimates of the error ellipsoids.

In HYPOCENTER, error ellipsoids are constructed through the variance scale factor (Jordan & Sverdrup 1981; Lienert & Havskov 1995), *a posteriori* estimated by

$$\frac{k+|\hat{e}^0|^2}{k+n-m},$$

where k, the number of degrees of freedom, is allowed to vary continuously from zero to infinity ($k=0$ when the variance scale factor is estimated *a posteriori* and $k=\infty$ when the variance scale factor is perfectly known *a priori*), n is the number of observed arrival times, m is the number of event parameters to be determined ($m=4$ for a full solution) and $\hat{e}^0$ is the residual between the observed data and the computed values.

When the covariance matrix is not diagonal, Lahr (1978) observed that the total error can be underestimated. In fact, the diagonal elements of the covariance matrix define the intersection points of the error ellipse with the x-, y- and z-axes. Thus, reliable projections of the error ellipsoids can be obtained by computing the eigenvalues and eigenvectors of covariance matrices.

The projections of the error ellipsoids presented in Fig. 3 are therefore computed (for the NBCI velocity structure) as follows:

(a) assuming an *a priori* residual in arrival times equal to 0.05 s (for a weight of 1);

(b) taking k equal to 50, which is equivalent to assuming an *a priori* error of 10 per cent in the variance scale factor (Jordan & Sverdrup 1981);

(c) considering the non-diagonal elements of the covariance matrices.

Fig. 3 and Table 5 show that error ellipsoids, when they are not underestimated, can be quite big when the distance to the nearest station is large. These results remind us that the fault plane solutions presented in this article are coarse results. Refined focal solutions could be obtained by constraining hypocentral depths by waveform modelling. This modelling will be possible when more information is available about the propagation medium.

4 TECTONICS AND HISTORICAL SEISMIC BACKGROUND

The structural regime of Normandy is characterized by the occurrence of two sets of faults striking NW–SE and ENE–WSW (Wynns 1977; Dupret *et al*. 1990; Chantraine *et al*. 1996; Baize *et al*. 1998) (Fig. 3). The distribution of the regional instrumental seismicity has already been studied in a previous paper. Several of the regional main faults are considered to be seismically active (Amorèse *et al*. 1999). On Jersey, the principal faults follow three main trends N–S, NW–SE and NE–SW (Walker 1991).

Hereafter, 'MM' stands for macroseismic magnitude. As this value is a crude estimate of the instrumental magnitude, we note its decimal part in fraction form.

The area of the Channel Islands is of particular seismotectonic interest because it experienced two MM = 5 1/4 earthquakes in 1926 and 1927 (Levret *et al*. 1996). They were located between the east of Jersey and the Normandy coast. The largest one, in 1926, caused significant structural damage to the upper parts of buildings (Mourant 1933). The western part of the Cotentin peninsula, near Coutances, also experienced a slightly damaging MM = 5 3/4 earthquake in 1853 (Levret *et al*. 1996).

In other respects, the historical seismicity under Normandy is not restricted to the area of the Gulf of Saint-Malo: the 1775 Caen earthquake (Lambert *et al*. 1996) and the 1889 MM = 5 1/2 Cherbourg earthquake (Levret *et al*. 1996) are two other strong historical earthquakes (with maximum intensities greater than or equal to VI MSK) that have occurred in the area of investigation.

In total, 25 events with an epicentral MSK intensity greater than or equal to V are reported to have occurred in the studied area since 1241 (Lambert *et al*. 1996).

5 RESULTS

Hereafter, a low quality rating is assigned to focal mechanisms showing multiple solutions. The map of all the fault plane solutions (Fig. 4) that we computed (Table 5) for earthquakes in Normandy shows a complicated pattern. Details of all the computed fault plane solutions are plotted in the Appendix.

5.1 Normal faulting

Many dominantly normal faulting events are shown in Fig. 4. The Arromanches and Saint-Brieuc earthquakes show normal fault plane solutions. For the Arromanches earthquake, two

Downloaded from https://academic.oup.com/gji/article/143/3/837/721582 by guest on 10 January 2021

© 2000 RAS, *GJI* **143,** 837–846

Downloaded from https://academic.oup.com/gji/article/143/3/837/721582 by guest on 10 January 2021

Table 5. Hypocentral parameters and fault plane solutions. Reported origin time, latitude, longitude, depth, RMS, nearest station distance and error values are computed with the preferred (NBCI) structure. Δh and Δz are not the usual Erh and Erz values. Δh is the length of the semi-major axis of the projected 90 per cent confidence ellipsoid on the horizontal plane. Δz is the vertical gap between the hypocentre and the deepest point of the 90 per cent confidence ellipsoid. Z is the focal depth (when the NBCI and the BGS velocity models provide different depth values, the Z column includes, first, the value computed using the NBCI model and, second, the value computed using the BGS model). M_L is the local magnitude computed by the LDG. Dn is the epicentral distance to the nearest station. Δ is the angle uncertainty on the nodal plane (this value is determined from the maximum half-widths of 90 per cent confidence ranges of strike, dip and rake values computed by FPFIT). N is the number of first-motion observations used in fault plane solution. Mis is the solution misfit value. STDR is the station distribution ratio. In the case of multiple solutions, adopted mechanisms are marked by daggers. Alternative fault plane solutions obtained with the BGS velocity model are marked by double daggers. The 1990 April 30 event is marked by an asterisk because a fault plane solution has already been published for this event (Walker 1991). For this event, the M_L value is the magnitude computed by Walker (1991).

Date (Mo/Dy/Yr)	Time	Lat. (°)	Lon. (°)	Δh (km)	Z (km)	Δz (km)	M_L	RMS (s)	Dn (km)	Location	Plane 1			Plane 2			P axis		T axis		N/Mis/STDR
											Φ_s (°)	δ (°)	Δ (°)	Φ_s (°)	δ (°)	Δ (°)	Az (°)	Pl (°)	Az (°)	Pl (°)	
04/30/1990*	23:35:57.2	49.105	−2.172	2	8	3	3.5	0.29	9	Jersey	35	75	10	215	15	17	305	60	125	30	29/0.07/0.77†
											15	90	11	285	45	11	250	30	140	30	29/0.10/0.78‡
											35	70	11	215	20	15	305	65	125	25	29/0.07/0.78‡
											0	10	5	240	85	13	322	39	160	49	29/0.10/0.72‡
11/08/1990	18:21:47.4	48.457	−1.387	5	13	8	3.0	0.55	40	Pontorson	15	58	10	230	36	22	121	11	246	71	15/0.00/0.63†
											18	57	12	232	38	25	122	10	242	70	15/0.00/0.68‡
07/26/1993	18:52:21.9	48.823	−1.165	10	12, 10	29	3.5	0.48	51	SW Vire	88	17	6	301	76	6	24	30	224	58	20/0.10/0.39
											115	45	10	227	69	31	346	14	93	49	20/0.10/0.50‡†
09/17/1994	06:05:03.5	49.015	−2.700	8	8	6	3.4	0.32	42	W Minquiers	25	85	30	117	70	17	339	18	72	10	9/0.00/0.79
											305	90	6	215	70	36	172	14	78	14	9/0.00/0.78‡
											160	35	10	340	55	20	250	80	70	10	9/0.00/0.77‡†
11/30/1994	16:31:21.5	49.437	−0.577	5	14	8	4.1	0.45	75	Arromanches	105	25	5	328	71	13	262	60	45	24	17/0.08/0.42†
											40	15	18	310	90	0	234	43	25	43	17/0.12/0.50‡
04/22/1995	13:10:13.3	48.698	−2.372	4	5, 8	6	3.5	0.21	56	Saint-Brieuc	95	75	9	330	25	11	340	56	201	27	13/0.03/0.54
											150	85	11	54	40	13	271	29	25	37	13/0.06/0.51
											95	75	9	330	25	11	340	56	201	27	13/0.03/0.55‡†
											165	70	9	44	35	10	277	19	37	55	13/0.06/0.47‡
06/01/1996	12:29:23.6	49.365	−1.367	3	13, 11	3	3.0	0.29	52	Saint-Lô	70	85	9	336	50	9	301	31	196	23	10/0.10/0.47
											20	30	13	268	78	48	336	28	208	50	10/0.20/0.64‡
											125	70	8	35	90	22	348	14	82	14	10/0.10/0.52‡†
											335	90	5	65	25	8	268	40	42	40	10/0.20/0.48‡
11/26/1996	20:21:35.5	48.704	−1.555	4	10, 11	11	3.9	0.38	62	Avranches	105	65	10	1	63	14	324	38	233	1	19/0.05/0.64†
											90	55	5	348	74	14	303	37	43	12	19/0.05/0.59‡
06/22/1997	16:50:16.4	49.204	−2.273	3	13, 11	3	3.4	0.42	5	Jersey	355	85	32	256	30	45	236	42	110	33	16/0.14/0.88
											40	85	8	139	30	10	338	42	105	33	16/0.14/0.65
											285	80	6	19	70	21	240	21	333	7	16/0.07/0.57†
											18	58	12	282	81	8	235	29	334	15	16/0.16/0.56‡
08/08/1998	10:36:16.2	49.287	−0.560	6	8, 11	8	3.5	0.37	15	Caen	70	13	9	281	79	26	5	33	199	56	18/0.06/0.63
											91	85	1	339	13	3	348	49	192	39	18/0.00/0.54†
											75	10	8	280	81	20	7	36	195	54	18/0.06/0.62‡
											90	85	9	315	7	18	354	50	185	40	18/0.00/0.54‡
12/07/1998	00:23:28.1	48.647	−1.680	2	5, 10	6	3.3	0.37	67	Avranches	175	80	9	277	41	14	122	41	235	24	20/0.05/0.74
											20	85	19	276	21	13	128	37	269	46	20/0.05/0.74
											150	55	5	313	36	5	94	77	233	9	20/0.00/0.56‡†
											50	60	10	297	56	18	173	2	265	48	20/0.05/0.53‡

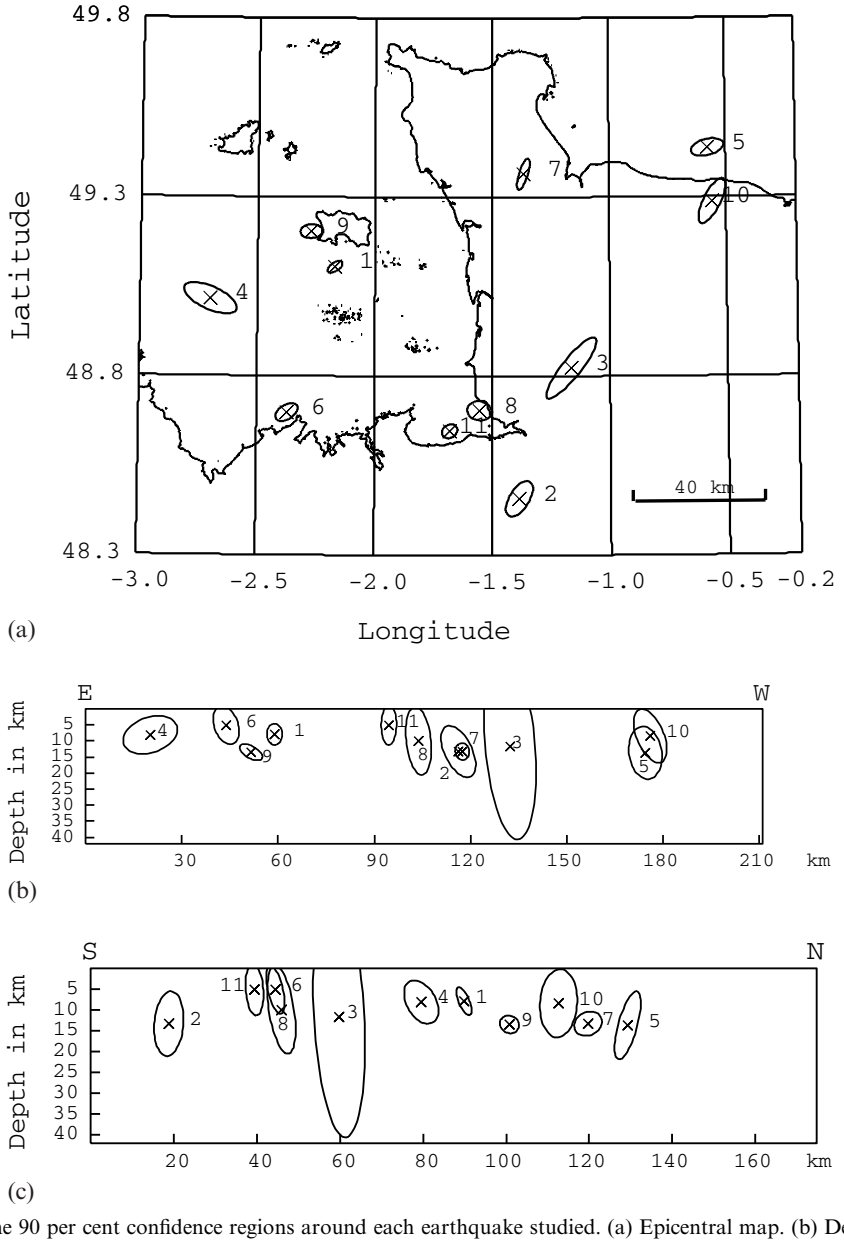

Figure 3. Projections of the 90 per cent confidence regions around each earthquake studied. (a) Epicentral map. (b) Depth profile along the E–W direction. (c) Depth profile along the S–N direction.

different solutions are obtained depending on the velocity structure used (NBCI or BGS). We adopt the focal mechanism obtained with the NBCI velocity structure because this solution shows the smallest misfit value. As the station distribution ratio (STDR) of this solution is small (less than 0.50), we assign to it a low quality rating (filled quadrants of the focal mechanism are shaded with grey in Fig. 4). For the Saint-Brieuc earthquake, four possible solutions are computed by FPFIT (Table 5). The best one, showing the smallest misfit value and the largest STDR value, is the first focal mechanism obtained with the BGS velocity structure. The Arromanches and Saint-Brieuc earthquakes show T-axes trending N45°E and N201°E (Table 5), respectively.

Apparently, three fault plane solutions are possible for the event that occurred to the west of the Minquiers Islands (Table 5). These solutions show T-axis trends varying from N70°E to N78°E. We adopt the second focal mechanism computed with the BGS velocity structure (Table 5 and Fig. 4). This fault plane solution is selected because it looks like the one computed for the nearby Saint-Brieuc event. This choice is biased and the polarities are unevenly distributed on the sphere, so a low quality rating is assigned to the fault plane solution of the Minquiers earthquake.

Fault plane solutions computed for the 1990 April 30 Jersey event show a good compatibility (the minimum SC value is equal to 0.68 in Table 4). Our preferred solution for this seismic event is a normal faulting solution with a T-axis trend angle near N125°E. We prefer this focal mechanism principally because the same solution is obtained using both the NBCI and the BGS velocity models (it also shows the smallest misfit value).

Several focal solutions are possible for the 1998 Avranches earthquake (Table 5). The best is the first fault plane solution

Downloaded from https://academic.oup.com/gji/article/143/3/837/721582 by guest on 10 January 2021

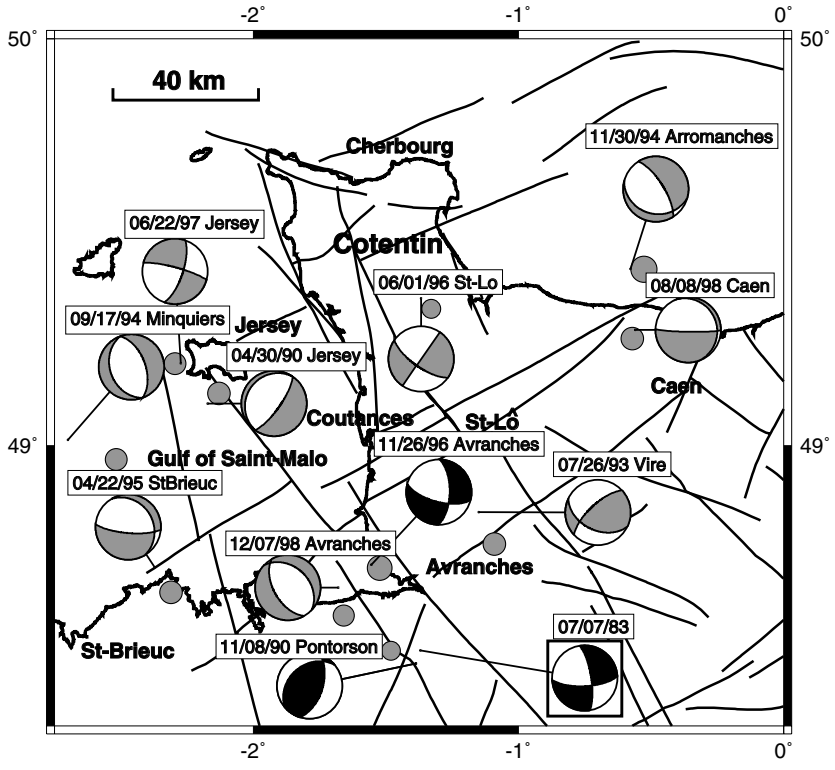

Figure 4. A summary of the fault plane solutions. Filled circles are initial epicentre locations (see Table 1). Lines are plotted between relocated epicentres and focal mechanisms. Focal mechanisms with filled black quadrants are high-quality solutions. Focal mechanisms with filled grey quadrants refer to low-quality solutions. Heavy lines are regional faults (Baize *et al.* 1998). The 1983 July 7 earthquake fault plane solution (in a box in the SE corner of the figure) is from Delouis *et al.* (1993).

obtained with the BGS velocity structure because it shows a null misfit value. This solution is also a good candidate because of its consistency with a NE–SW T-axis trend as inferred from the 1996 Avranches earthquake. The 1998 Avranches earthquake is apparently located on a NNW–SSE fault zone (Fig. 4). On this fault, the focal mechanism of the 1998 Avranches earthquake implies normal motion. The quality of the fault plane solution of the 1998 Avranches earthquake is low (multiple solutions exist).

For the Caen earthquake, as it shows a null misfit value, we adopt the second fault plane solution obtained with the NBCI velocity model. This focal mechanism implies a N–S T-axis trend and is inconsistent with the apparent regional stress pattern. This fault plane solution is, however, a low-quality result (multiple solutions).

5.2 Thrust faulting

The focal mechanism that has been determined for the Pontorson earthquake is well constrained (Tables 4 and 5). It represents an almost pure thrust faulting mechanism with a P-axis trending N121°E. The strikes of the nodal planes are approximately NE–SW. Dominant thrust faulting is also suggested by a relatively poorly controlled fault plane solution computed for an event near Vire (Table 5 and Fig. 4). For this event, depending on the used velocity structure, two alternative solutions are proposed (Table 5). The P-axis trend angle N346°E inferred from the focal mechanism associated with the BGS velocity structure seems to be consistent with the regional P-axis trend (as inferred from the Pontorson or the 1996 Avranches earthquake). This suggests that the solution obtained with the BGS velocity structure is more likely. The fault plane solution of the Vire earthquake is assigned a low quality rating. Independently of multiple fault plane solutions, this focal mechanism should be regarded with caution as its hypocentral depth is very poorly constrained (Table 5).

5.3 Strike-slip faulting

The focal mechanism of the 1996 Avranches earthquake is a well-constrained strike-slip solution showing a significant normal component (Tables 4 and 5 and Fig. 4). The P- and T-axis trends are, respectively, N324°E and N233°E. The fault plane solution of the 1996 Avranches earthquake is similar to that obtained by joint inversion of the stress tensor and fault plane solutions for the Fougères earthquake (Delouis *et al.* 1993). For the Saint-Lô earthquake, our preferred solution is the focal mechanism showing the smallest misfit value and the largest STDR value. This low-quality solution (minimum SC value equal to 0.45 in Table 4), computed with the BGS velocity structure, shows a P-axis trending N348°E and a T-axis trending N82°E (Fig. 4).

The diversity of focal solutions is particularly great for the 1997 Jersey event (minimum SC value is equal to 0.40 in Table 4). Our preferred solution is the third focal mechanism computed with the NBCI velocity structure because this solution shows the smallest misfit value. This fault plane solution is assigned a low quality rating (multiple solutions).

Downloaded from https://academic.oup.com/gji/article/143/3/837/721582 by guest on 10 January 2021

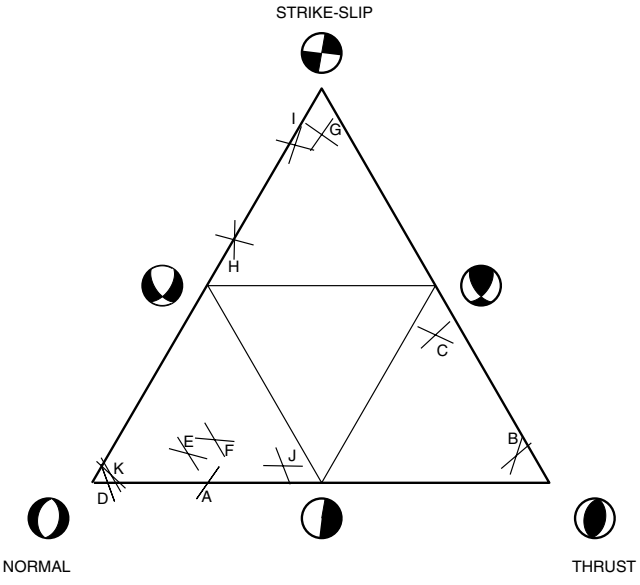

Figure 5. A ternary plot of the fault plane solutions. Strikes of the nodal planes are plotted. Earthquakes are as follows: A, 1990 Jersey earthquake; B, Pontorson earthquake; C, Vire earthquake; D, W Minquiers earthquake; E, Arromanches earthquake; F, Saint-Brieuc earthquake; G, Saint-Lô earthquake; H, 1996 Avranches earthquake; I, 1997 Jersey earthquake; J, Caen earthquake; K, 1998 Avranches earthquake).

6 DISCUSSION AND CONCLUSIONS

For continental areas, the interpretation of fault plane solutions of small earthquakes is not straightforward and should be conducted cautiously. In these areas, since minor faulting with no relation to the regional stress can occur, small earthquakes that are not representative of the regional stress field are also possible (Jackson 1983). When considered individually, a fault plane solution (for a small earthquake) cannot lead to a reliable interpretation. In fact, stress directions obtained using the P- and T-axes of an individual focal mechanism for a small earthquake can be in error by 30°–40° (McKenzie 1969; Zoback & Zoback 1980). It is difficult to produce a comprehensive interpretation of fault plane solutions for the area owing to the quality and size of the data set (11 events). Our purpose is just to highlight the apparent coarse features of stress and strain regimes in western Normandy.

Fault plane solutions of small intraplate earthquakes in Normandy show diverse styles of faulting and deformation, and a comprehensive discussion of the results is facilitated by using Fig. 5. Solutions with near-horizontal T-axes, and particularly normal solutions, are predominant; except for Jersey's earthquakes, normal and strike-slip faulting mechanisms (D, E, F, G, H, J, K in Fig. 5) show T-axes consistently oriented roughly N–S to NE–SW (Table 5). Except for the 1997 Jersey earthquake, from strike-slip and thrust solutions (B, C, H in Fig. 5) it seems that when P-axes are near-horizontal, they strike roughly NW–SE. These results agree with the stress pattern in western Britain: the regional direction of the axis of maximum compression is N315° in Cornwall and N338° in North Wales (Ritchie & Walker 1991). In the same way, minimum axes of compression are horizontal and oriented, respectively, NE–SW and ENE–WSW in Cornwall and North Wales (Ritchie & Walker 1991).

The nodal planes of our 11 fault plane solutions for Normandy do not appear to be randomly oriented. Nodal planes of solutions showing large components of normal faulting commonly strike roughly NW–SE or E–W, and those with large components of thrust faulting commonly strike roughly NE–SW. The juxtaposition of normal and thrust faulting along roughly perpendicular directions is likely to be indicative of a strike-slip stress regime. Statistically, any conclusions made from our observations are weak because of the small data set. Nevertheless, for Normandy, such a global strain pattern is consistent with geological and geomorphological observations (Lagarde *et al.* 2000). Our results can be compared to the stress pattern determined by Delouis *et al.* (1993) in the Central and Armorican Massifs. These authors obtained an extensional but close to strike-slip stress pattern with σ_3 oriented N35°E.

The 1990 Jersey earthquake presents a unique focal mechanism. This normal fault plane solution has NE-trending nodal planes. This is not in agreement with the regional strain pattern suggested earlier. In the same way, this solution does not agree with the focal mechanism previously computed by Walker (1991). Two possible explanations are suggested: (i) the computation is performed with errors in polarity data or (ii) the 1990 Jersey earthquake merely indicates a local stress readjustment that is not representative of the regional stress field. The 1997 Jersey earthquake also shows a singular focal mechanism (Fig. 3), but in this case it is probably due to the low stability of the fault plane solution (the minimum SC value is equal to 0.40 in Table 4).

The identification of the driving forces for earthquakes in Britain and Normandy is based on speculative assumptions. In agreement with the assumed stress orientations, both the NW–SE 'ridge push' (from the Mid-Atlantic Ridge system) (Marrow & Turbitt 1988; Gölke & Coblentz 1996) and the NW–SE 'Alpine push' (Bevan & Hancock 1986; Gölke & Coblentz 1996) are conceivable additive causes.

ACKNOWLEDGMENTS

We thank M. Nicolas (DASE/LDG), B. Simpson (BGS), Y. Ménéchal (DASE/LDG) and M. Granet (ReNaSS) for providing most of the data used in this study. A review by Marc Nicolas helped to clarify the article. The authors (especially DA) give special thanks to B. Lienert (HIGP/SOEST, University of Hawaii) for providing the error ellipse plotting program and for helpful E-mails. Acknowledgment is due to the BERSSIN/IPSN and the Conseil Régional de Basse-Normandie for the financial support of the Siscaen network. We are grateful to all of the people involved in the running of the Siscaen network: G. Guillemet and L. Benoit (M2C) for the maintenance and the CROSS Jobourg, Sémaphore de Port-en-Bessin and Lycée du Robillard for sheltering the seismic stations. Maps were drawn using GMT (Wessel & Smith 1991). This paper is contribution no. 78 of the GéoFrance 3D programme.

REFERENCES

Amorèse, D., Lagarde, J.-L. & Laville, E., 1999. A point pattern analysis of the distribution of earthquakes in Normandy (France), *Bull. seism. Soc. Am.,* **89,** 742–749.

Baize, S., Lagarde, J.-L., Laville, E. & Dugué, O., 1998. Géomorphologie d'un plateau littoral (Cotentin—Normandie): enregistrements des signaux tectoniques et climatiques, *Bull. Soc. Géol. Fr.,* **169,** 851–866.

Downloaded from https://academic.oup.com/gji/article/143/3/837/721582 by guest on 10 January 2021

Bevan, T.G. & Hancock, P.L., 1986. A late Cenozoic regional mesofracture system in southern England and northern France, *J. geol. Soc. Lond.,* **143,** 355–362.

Buland, R., 1976. The mechanics of locating earthquakes, *Bull. seism. Soc. Am.,* **66,** 173–187.

Chantraine, J., Autran, A. & Cavelier, C., 1996. *Carte Géologique de la France au 1/1000000*, 6ème édn, BRGM, Orléans, France.

Delouis, B., Haessler, H., Cisternas, A. & Rivera, L., 1993. Stress tensor determination in France and neighbouring regions, *Tectonophysics,* **221,** 413–438.

Dupret, L., Dissler, E., Doré, F., Gresselin, F. & Le Gall, J., 1990. Cadomian geodynamic evolution of the Northeastern Armorican Massif (Normandy and Maine), in *The Cadomian Orogeny,* eds D'Lemos, R.S., Strachan, R.A. & Topley, C.G., *Geol. Soc. Spec. Publ.,* **51,** 115–131.

Gölke, M. & Coblentz, D., 1996. Origins of the European regional stress field, *Tectonophysics,* **266,** 11–24.

Grandjean, G., Guennoc, P., Recq, M. & Andréo, P., 2000. Refraction/wide angle reflection investigation of the Cadomian crust between northern Brittany and the Channel Islands, *Tectonophysics,* in press.

Grellet, B., Combes, P., Granier, T. & Philip, H., 1993. Sismotectonique de la France métropolitaine, *Mem. Soc. Géol. Fr.,* **164,** Soc. géol. France, Paris.

Jackson, J.A., 1983. The use of earthquake source studies in continental tectonic geology, in *Terremoti: Osservazione, Teoria E Interpretazione, Scuola Internazionale Di Fisica 'Enrico Fermi', Societa Italiana Di Fisica, Bologna,* pp. 456–478, eds Kanamori, H. & Boschi, E., North Holland, Amsterdam.

James, D.E., Sacks, I.S., Lazo, L.E. & Aparicio, P.G., 1969. On locating local earthquakes using small networks, *Bull. seism. Soc. Am.,* **59,** 1201–1212.

Jordan, T.H. & Sverdrup, K.A., 1981. Teleseismic location techniques and their application to earthquake clusters in the south-central Pacific, *Bull. seism. Soc. Am.,* **71,** 1105–1130.

Lagarde, J.-L., Baize, S., Amorèse, D., Delcaillau, B., Font, M. & Volant, P., 2000. Active tectonics, seismicity and geomorphology with special reference to Normandy (France), *J. Quat. Sci.,* in press.

Lahr, J.C., 1978. HYPOELLIPSE: A computer program for determining local earthquake hypocentral parameters, magnitude, and first motion pattern, *USGS Open File Rept,* USGS, Menlo Park, CA.

Lambert, J., Levret-Albaret, A., Cushing, M. & Durouchoux, C., 1996. *Mille Ans de Séismes en France,* Ouest Editions, Nantes, France.

Levret, A., Cushing, M. & Peyridieu, G., 1996. *Etude des Caractéristiques de Séismes Historiques en France, Atlas de 140 Cartes Macrosismiques,* Institut de Protection et de Sûreté Nucléaire, Fontenay-Aux-Roses, France.

Lienert, B.R., 1997. Assessment of earthquake location accuracy and confidence region estimates using known nuclear tests, *Bull. seism. Soc. Am.,* **87,** 1150–1157.

Lienert, B.R. & Havskov, J., 1995. A computer program for locating earthquakes both locally and globally, *Seism. Res. Lett.,* **66,** 26–36.

Lienert, B.R., Berg, E., Frazer, L. & N., 1986. HYPOCENTER: an earthquake location method using centered, scaled, and adaptively least squares, *Bull. seism. Soc. Am.,* **76,** 771–783.

Marrow, P.C. & Turbitt, T., 1988. Earthquake source mechanisms and principle stress orientations in Britain and NW Europe, *Geophys. J.,* **92**.

Matte, P. & Hirn, A., 1988. Seismic signature and tectonic cross section of the Variscan crust in western France, *Tectonics,* **7,** 141–155.

McKenzie, D.P., 1969. The relation between fault plane solutions for earthquakes and the directions of principal stresses, *Bull. seism. Soc. Am.,* **59,** 591–601.

Mourant, A.E., 1933. *Earthquakes of the Channel Islands and Neighbouring Countries: a Seismological and Historical Account,* J. T. Bigwood, Jersey.

Nicolas, M., Santoire, J.P. & Delpech, P.Y., 1990. Intraplate seismicity: new seismotectonic data in western Europe, *Tectonophysics,* **179,** 27–53.

Nordquist, J.M., 1962. A special-purpose program for earthquake location with an electronic computer, *Bull. seism. Soc. Am.,* **52,** 431–437.

Reasenberg, P.A. & Oppenheimer, D., 1985. FPFIT, FPPLOT and FPPAGE: Fortran computer programs for calculating and displaying earthquake fault-plane solutions, *USGS Open File Rept,* **85–739**.

Ritchie, M.E.A. & Walker, A.B., 1991. Focal mechanisms and the determination of stress directions in western Britain, *BGS Global Seismology Rept,* **WL/91/22**.

Walker, A.B., 1991. The Jersey earthquake of 30 April, 1990, *Ann. Bull. Soc. Jersiaise,* **25,** 529–538.

Wessel, P. & Smith, W.H.F., 1991. Free software helps map and display data, *EOS, Trans. Am. geophys. Un.,* **72,** 445–446.

Wynns, R., 1977. Tectonique récente dans l'Ouest du bassin de Paris: méthodes d'étude et bilan des déformations plio-quaternaires, *Bull. Soc. Géol. Fr.,* **7,** 1093–1101.

Zoback, M.L. & Zoback, M.D., 1980. State of stress in the conterminous United States, *J. geophys. Res.,* **85**(B11), 6113–6156.

Downloaded from https://academic.oup.com/gji/article/143/3/837/721582 by guest on 10 January 2021

APPENDIX A: PLOTS OF ALL THE FOCAL MECHANISMS COMPUTED IN THIS STUDY

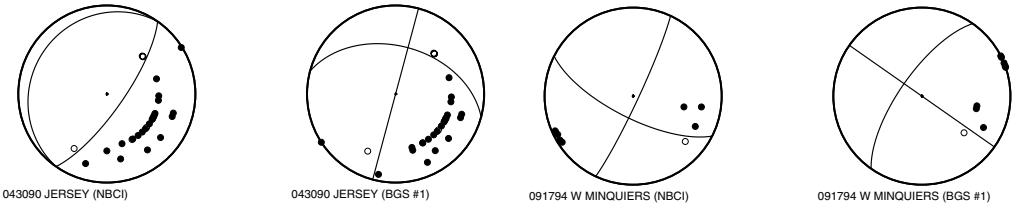

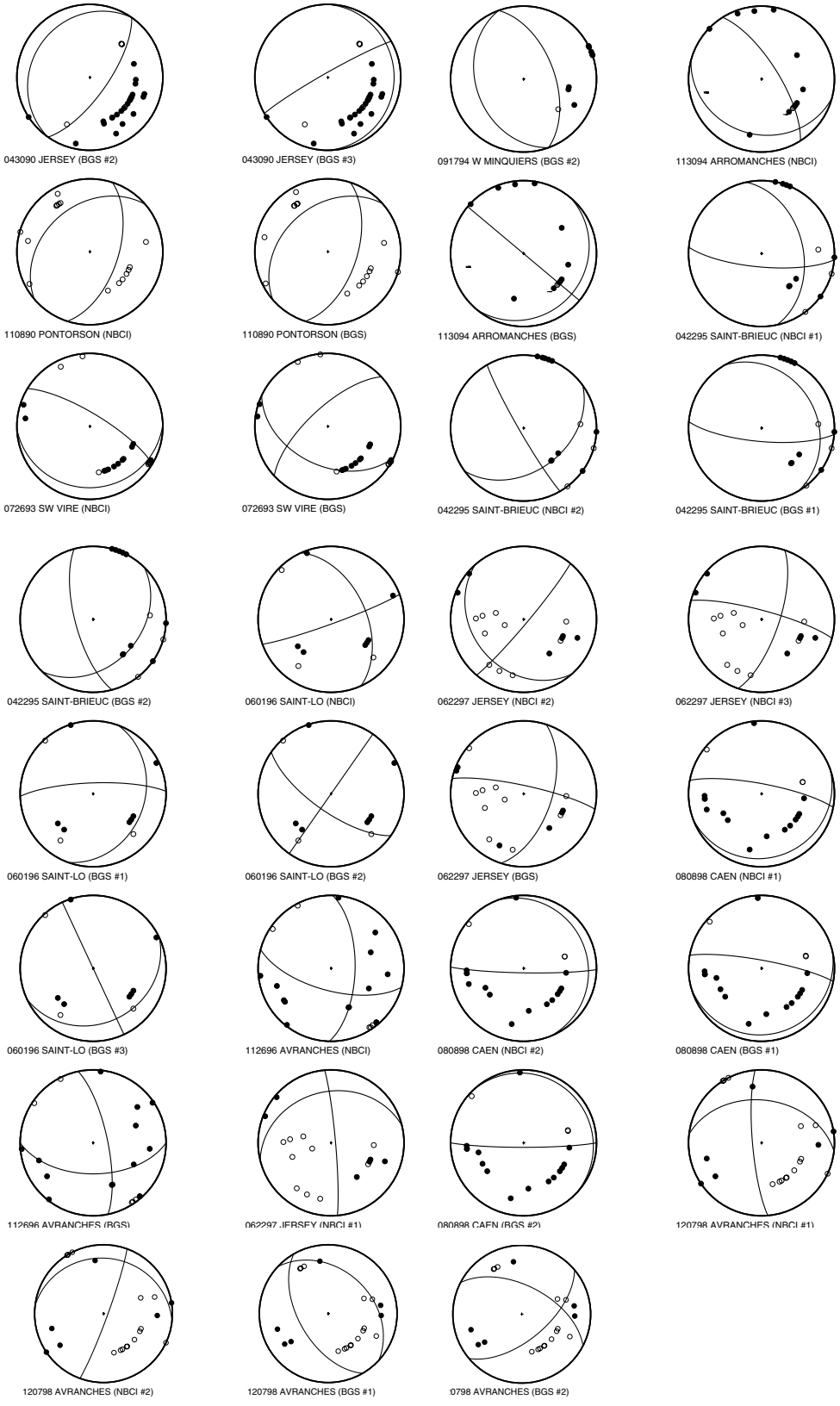

Downloaded from https://academic.oup.com/gji/article/143/3/837/721582 by guest on 10 January 2021